REPORT

PHYSICS

Metastable ferroelectricity in optically strained $SrTiO_3$

T. F. Nova[1,2]*, A. S. Disa[1], M. Fechner[1], A. Cavalleri[1,2,3]*

Fluctuating orders in solids are generally considered high-temperature precursors of broken symmetry phases. However, in some cases, these fluctuations persist to zero temperature and prevent the emergence of long-range order. Strontium titanate ($SrTiO_3$) is a quantum paraelectric in which dipolar fluctuations grow upon cooling, although a long-range ferroelectric order never sets in. Here, we show that optical excitation of lattice vibrations can induce polar order. This metastable polar phase, observed up to temperatures exceeding 290 kelvin, persists for hours after the optical pump is interrupted. Furthermore, hardening of a low-frequency vibration points to a photoinduced ferroelectric phase transition, with a spatial domain distribution suggestive of a photoflexoelectric coupling.

Strontium titanate ($SrTiO_3$) is paraelectric and centrosymmetric at all temperatures. When cooled, it displays many anomalies that suggest its proximity to a ferroelectric phase, including a large rise in the dielectric function (*1*) and softening of a polar mode (*2*). This behavior is often referred to as incipient ferroelectricity, with quantum fluctuations of the ionic positions preventing long-range ordering (*3*, *4*). The proximity to a ferroelectric phase is underscored by the ease with which $SrTiO_3$ can be made ferroelectric, for example, by Ca-substitution [Sr → Ca; Curie Temperature (T_c) = 37 K] (*5*) or by isotope substitution ($^{16}O \rightarrow {}^{18}O$; T_c = 25 K) (*6*). Strain, as shown in the phase diagram of Fig. 1, has proven most effective in controlling the transition in $SrTiO_3$ (*7*), with reported ferroelectricity up to room temperature (*8*).

Strong lattice deformations can also be achieved by irradiation with strong mid-infrared optical pulses (see Fig. 1), which can be made resonant with a specific lattice vibration in $SrTiO_3$. Nonlinear phonon excitation (*9*–*11*) may induce a polar or ferroelectric phase in many ways. For example, dynamical softening (*12*, *13*) of the polar mode by cubic lattice nonlinearities (*14*) or the generation of transiently induced strain [see supplementary text S11 in (*15*)] may all provide routes to creating a ferroelectric order absent at equilibrium.

In the experiments reported here, the highest-frequency A_{2u} vibrational mode of $SrTiO_3$ was resonantly excited (at T = 4 K) with femtosecond mid-infrared optical pulses tuned to 15-μm wavelength (83-meV photon energy) derived from a 1-kHz repetition rate Ti:Sapphire laser, an optical parametric amplifier, and a difference frequency mixing crystal (fig. S1). The optical polarization was aligned along the [001] axis of a (110)-oriented crystal (Fig. 2A).

$SrTiO_3$ was monitored through second harmonic generation (*16*) of a 2.2-μm wavelength optical probe pulse, colinear and time-delayed with respect to the mid-infrared pump (Fig. 2A). As shown in Fig. 2B, a time delay–independent second harmonic signal, absent at equilibrium, indicated the appearance of a noncentrosymmetric phase after mid-infrared excitation.

The second harmonic signal was observed to accumulate with exposure to mid-infrared radiation and reach saturation after several minutes, with a maximum value determined by the pump fluence (30 mJ/cm^2 for the data of Fig. 2B; see fig. S8 and supplementary text S6). As all other contributions to the second harmonic were negligible, including surface and quadrupole terms of the nonlinear susceptibility tensor, this observation was a reliable reporter of a photoinduced phase with broken inversion symmetry (supplementary text S3C).

Structural symmetry information was obtained by continuously rotating the incoming 2.2-μm probe polarization and measuring the 1.1-μm second harmonic projected along the pseudocubic [1 −10] and [001] crystallographic directions with a second polarizer (Fig. 2C). These angular dependences indicate the formation of a polarization along the [1 −10] direction and are consistent with a (noncentrosymmetric) polar point group (C_{2v}) (supplementary text S3B).

The experiment was performed as a function of sample temperature and pump wavelength. The induced second harmonic signal was found to be maximum at low temperatures but remained detectable up to room temperature (fig. S4 and supplementary text S4). In addition, the polar state was found to be most efficiently created when pumping resonantly with the A_{2u} phonon, whereas for pump photons in the proximity of the 3.2-eV bandgap of $SrTiO_3$, the effect

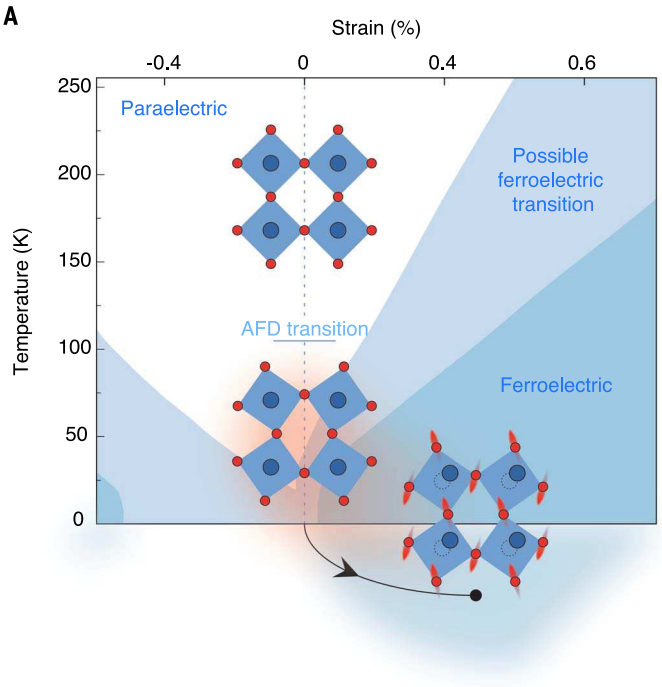

Fig. 1. Dynamical ferroelectricity in $SrTiO_3$. Bulk, unstrained $SrTiO_3$ is paraelectric at any finite temperature. At 105 K, it undergoes an antiferrodistortive (AFD) transition from cubic to tetragonal, although it retains a centrosymmetric structure. However, small amounts of strain cause the material to undergo a ferroelectric transition. The Curie temperature increases with growing values of applied strain, highlighting the paramount role of acoustic lattice deformations in controlling the transition. The strain-phase diagram shown here represents a thermodynamic analysis of the phase transition for a single-domain state, adapted from (*32*). The shaded cartoon explores the possibility of dynamically establishing a ferroelectric phase through vibrational excitation.

[1]Max Planck Institute for the Structure and Dynamics of Matter, Hamburg 22761, Germany. [2]The Hamburg Centre for Ultrafast Imaging, Hamburg 22761, Germany. [3]Clarendon Laboratory, University of Oxford, Oxford OX1 3PU, United Kingdom.
*Corresponding author. Email: tobia.nova@mpsd.mpg.de (T.F.N.); andrea.cavalleri@mpsd.mpg.de (A.C.)

disappeared (Fig. 2A, inset, and supplementary text S7).

The photoinduced phase was found to be metastable when unperturbed, relaxing back to the nonpolar equilibrium paraelectric phase only several hours after the pump was turned off (fig. S5). We found that the optically induced polar state could be reverted to the paraelectric ground state by exposing it to above-bandgap photons (>3.2 eV) (fig. S6) or by thermal cycling.

Figure 3 displays ultrafast measurements of the same second harmonic signal discussed above. In addition to the time delay–independent background shown in Fig. 2, visible as an offset in the traces of Fig. 3A, the second harmonic signal exhibited ultrafast oscillations that resulted from the pump-driven, impulsive, inelastic excitation of low-frequency polar modes (see Fig. 3A for three representative measurements taken after 10, 25, and 105 min of illumination).

The frequency of these oscillations increased visibly with the baseline second harmonic, as shown more comprehensively in Fig. 3B. The detected mode-hardening is reminiscent of the

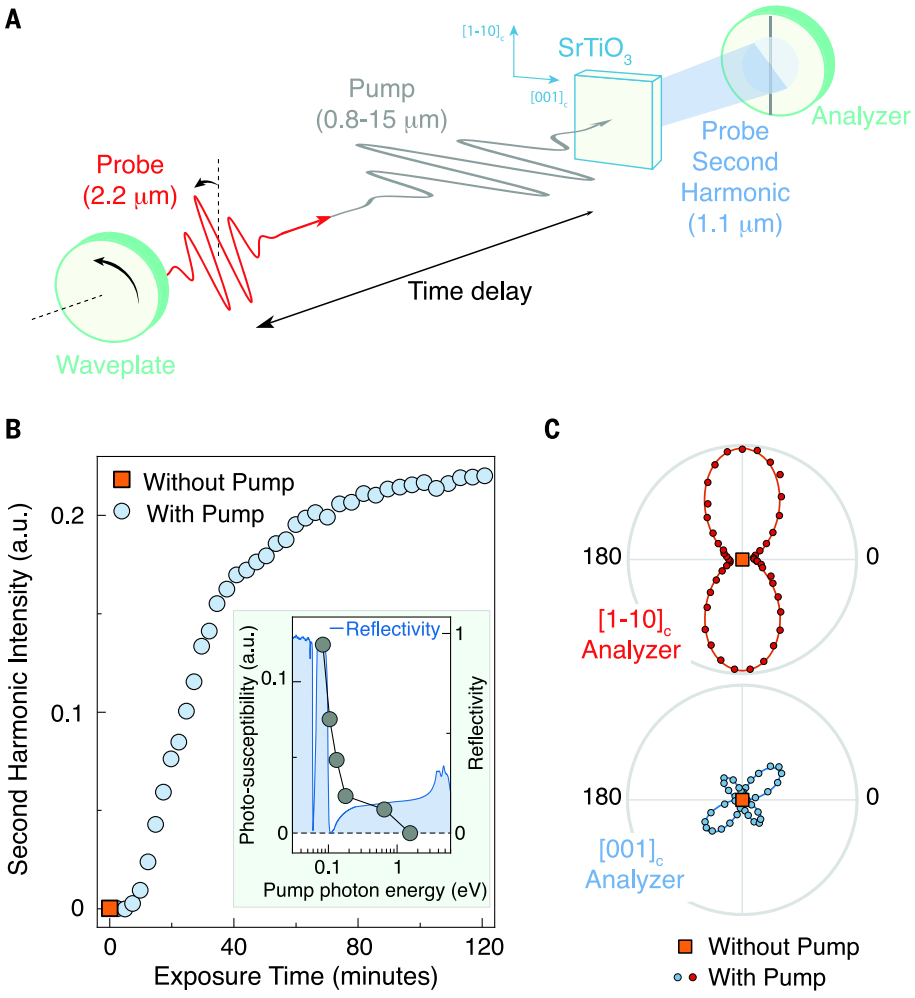

Fig. 2. A photoinduced polar state. (**A**) Sketch of the experimental setup. A (110)-oriented $SrTiO_3$ sample is coherently excited with tunable wavelength pulses (0.8 to 15 μm, gray line). Time-delayed colinear probe pulses (2.2-μm wavelength) impinge on the sample, with a half-waveplate controlling their polarization. The generated second harmonic (1.1 μm) is detected in transmission geometry. When needed, an analyzer (i.e., a polarizer) can be used to isolate orthogonal polarization components of the second harmonic. For a 15-μm wavelength pump, the full width at half maximum (FWHM) spot size was 72 μm. The probe was focused down to 52 μm FWHM. (**B**) Time delay–independent total second harmonic intensity impinging on the detector (without analyzer) as a function of exposure time to 15-μm pump pulses. a.u., arbitrary units. (**Inset**) Pump wavelength dependence. The gray dots represent the photosusceptibility of the effect, as defined in eq. S6.1 (see supplementary text S6 and S7). The data are compared with the static reflectivity of $SrTiO_3$ (blue line). The low-energy reflectivity data (< 0.2 eV) were measured by Fourier transform infrared spectroscopy (FTIR) with a commercial spectrometer. The high-energy data (>1 eV) were adapted from (*33*). (**C**) Second harmonic intensity in the saturated state as a function of the probe polarization for two orthogonal analyzer configurations.

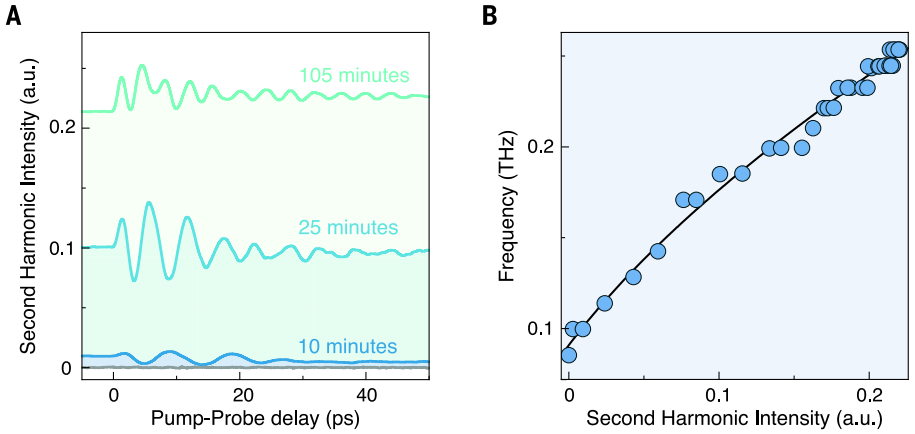

Fig. 3. Ferroelectric-like mode-hardening. (**A**) Pump-induced ultrafast modulation of the second harmonic intensity as a function of the pump-probe delay for different exposure times. The increasing offset corresponds to the delay-independent second harmonic of Fig. 2B. The gray line represents a measurement taken without mid-infrared pumping. No static second harmonic could be detected. (**B**) Frequency of the detected oscillations as a function of baseline second harmonic. The blue dots represent the frequency at which the Fourier spectrum of each ultrafast trace is maximum. The solid line is a guide to the eye.

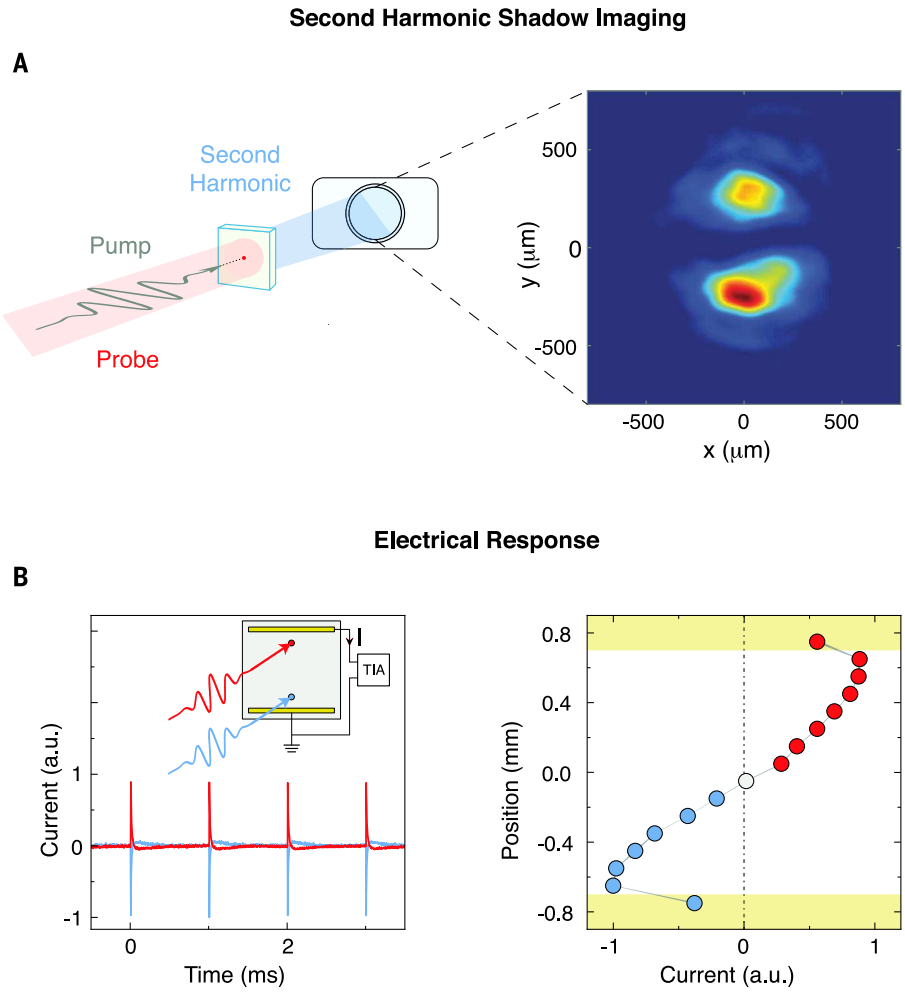

Fig. 4. A bipolar domain structure. (**A**) Second harmonic spatial dependence. (Left) Second harmonic shadow imaging setup. A collimated probe beam (1200 μm, much bigger than the 70-μm pump spot) uniformly illuminates the sample. The emitted second harmonic spatial profile is recorded with a CMOS camera (details in supplementary text S8). (Right) Measured second harmonic spatial dependence. (**B**) Electrical response. (Left) Electrical currents induced in $SrTiO_3$ by successive pump pulses (1-kHz repetition rate). The red and blue traces represent measurements taken with the pump impinging closer to the upper and lower contact, respectively. (**Inset**) Sketch of the transport measurements setup. Gold contacts were deposited on the sample surface, and the electrical response was recorded in short-circuit conditions without any applied bias. TIA, transimpedence amplifier (materials and methods S2). (Right) Maximum amplitude of the current pulses as a function of the pump position with respect to the contacts (yellow).

behavior of a ferroelectric soft mode across a paraelectric-to-ferroelectric phase transition (*17*–*19*).

To determine the spatial distribution of the photoinduced polar phase, we repeated the experiment with a collimated 2.2-μm probe beam that was made larger than the photoexcited spot. The second harmonic shadow of the transformed volume was projected onto a complementary metal-oxide semiconductor camera (Fig. 4A, left). Two oval bright regions with a dark area in the center were observed (Fig. 4A, right), indicative of an inhomogeneous polar state.

This inhomogeneity was further evidenced by electrical measurements (materials and methods S2). Gold contacts were deposited onto the sample surface, and the optical pump spot was kept much smaller (70-μm diameter) than the distance between the electrodes (1.5 mm). Measurements of the pump-induced electrical response were conducted under short-circuit conditions, without any applied bias (inset, Fig. 4B, left). Because the optically transformed region was far smaller than the gap between the electrodes, and because the electrodes themselves were not irradiated, the only coupling between the light-induced polar domains and the external circuit was capacitive. The ultrafast response was transmitted to the external circuit, in the form of short bursts of electrical currents at the 1-kHz repetition rate of the pump laser (Fig. 4B, left panel, red line).

The sign and amplitude of these current pulses were observed to be dependent on the position of the pump beam. No current pulses were detected when the pump pulse spot was in the middle of the gap (Fig. 4B, right), whereas currents of opposite sign (red and blue, Fig. 4B) were observed as the spot was moved toward either of the contacts.

The observations reported in Fig. 4 are indicative of the creation of two oppositely oriented polar domains in the pumped spot, which can be understood as follows.

First, oppositely oriented domains are expected to generate second harmonic light with equal intensities but with a relative π shift in their respective optical phases. Hence, as the two second harmonic beams propagated toward the detector, they destructively interfered in the center (Fig. 5C and fig. S11), resulting in the observed pattern (Fig. 5B). Second, upon excitation, each of the two domains is expected to draw currents in opposite directions from the electrodes because of the induced polarizations. For a pair of domains aligned at equal distances from the electrodes, no net current is anticipated. However, when these are moved in either direction, the two capacitances connecting each domain to the electrodes would become unequal, drawing a net current in either direction (Fig. 5D).

We next turn to a possible explanation for the formation of the two domains. We consider the dynamical equivalent of the ionic contribution to electrostriction. An optically pumped phonon mode coordinate Q_{IR} generates prompt stress (pressure) σ. Only hundreds of picoseconds after the femtosecond mid-infrared pulse, the stress is expected to evolve into transient strain (supplementary text S11). According to our estimates, pump peak field strengths of 18 MV/cm, predicted to induce ionic oscillations of 5-pm amplitude, result in a peak stress of 0.5 GPa. A 0.2% upper bound for the resulting transient strain is estimated (supplementary text S11). If we consider a strain profile with the same Gaussian shape of the pump beam, the pump-induced strain can generate a polarization in two ways. One can exclude a direct, strain-induced ferroelectric order, which would result in a single domain with polarization either up or down (Fig. 5A), a homogeneous second harmonic shadow, and monopolar current pulses (supplementary text S10). Rather, the coupling between the spatial gradient of the optical strain and polarization (Fig. 5B), arising from the flexoelectric effect (*20*, *21*), would result in the creation of two distinct, opposing polarizations and would readily explain the data of Fig. 4 (see Fig. 5, B to D, and supplementary text S10).

Although photoflexoelectricity appears to be a plausible explanation for the transient generation of polar domains, this hypothesis does not, per se, clarify the accumulation or metastability of the ferroelectric state.

It is possible that an ultrafast photoinduced polarization, triggered by the rapid formation of surface strain and subsequent flexoelectricity, would act on preexisting randomly distributed

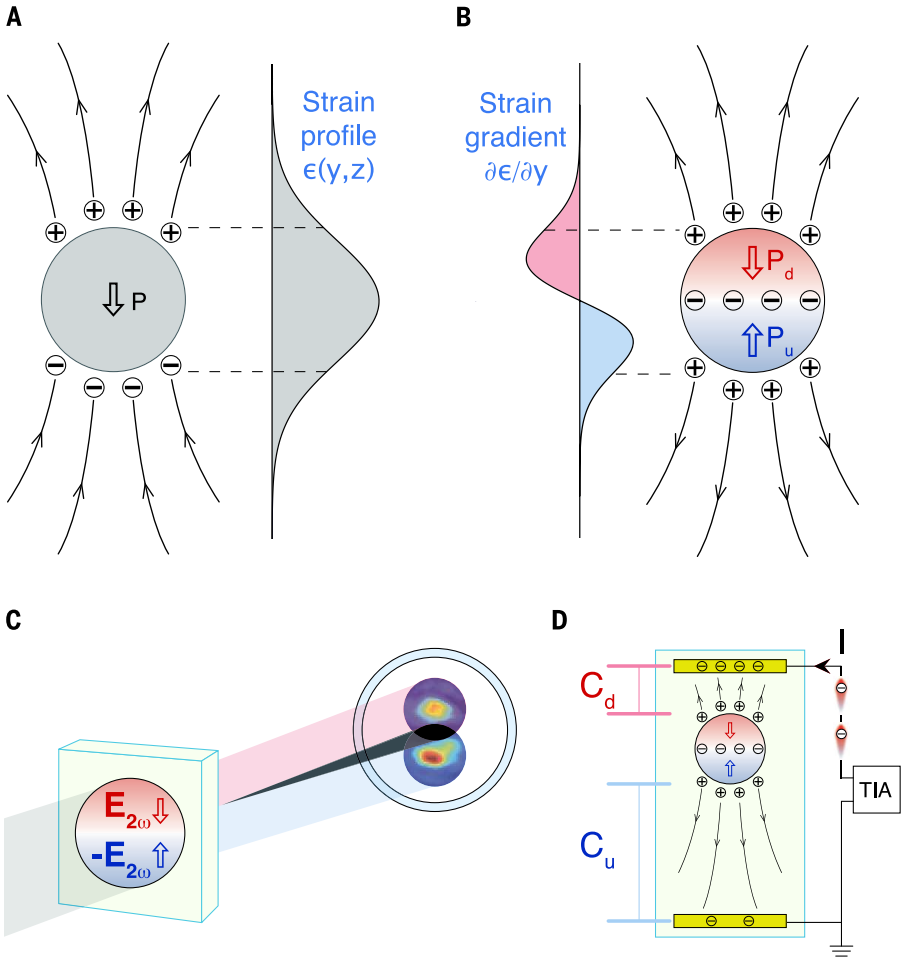

Fig. 5. Flexoelectric polarizations. (**A**) Phonon pumping results in a strain profile that follows the Gaussian profile of the pump beam (72-μm spot size FWHM). The figure depicts how a direct strain-induced transition to a ferroelectric monodomain state would look. (**B**) Inhomogeneous strain results in two distinct flexoelectric polarizations of opposite polarity that follow the strain gradient. (**C**) Two opposing polarizations generate antiphase second harmonic optical fields that interfere destructively on the CMOS camera (supplementary text S8 and S10). (**D**) The position of the flexoelectric domains with respect to the contacts determines the current amplitude and sign (supplementary text S10).

polar nanoregions (PNRs) (*22*). These may then align along a preferential direction. Owing to the transient nature of the aligning field and the intrinsically slow response time of the PNR, their alignment would only be partial after a single pulse. Subsequent pulses may facilitate the growth of macroscopic domains over a long incubation period, requiring tens of thousands of pulses. This hypothesis implies that in between two pulses, the induced partial alignment would not relax entirely to the unperturbed state—an assumption compatible with the known long relaxation times of PNRs (*22*).

An alternative explanation starts from photorefractivity (*23*, *24*). Impurity centers, which may lie in the energy range of the mid-infrared wavelengths used in this experiment, could be ionized concomitantly with the optically induced strain. The transient flexoelectric polarizations would force such photogenerated charges to slowly diffuse toward the edge of the excited area, where they eventually get trapped. However, all reported observations of photorefractivity take place for pump photon energies in the vicinity of the optical gap. In our experiment, on the contrary, the second harmonic signal progressively disappears for pump light approaching the optical gap of $SrTiO_3$. Overall, we regard this second hypothesis as less likely.

Our experimental results should motivate a new class of optical control experiments that rely on the perturbation of $SrTiO_3$ in functional materials. Because $SrTiO_3$ is used commonly as a substrate for the growth of oxide heterostructures, one could conceive of new ways to drive functional properties at interfaces (*25*, *26*)—including magnetic, electronic, and even superconducting states. Furthermore, the applicability of the optical control of flexoelectric polarizations extends far beyond the specific case of $SrTiO_3$, because flexoelectricity is allowed in materials of any symmetry (*20*, *21*).

More generally, our findings are a rare example of symmetry breaking by light and can thus be considered in the context of other types of light-induced phase transitions (*27*–*29*) in the presence of fluctuating order above the thermodynamic transition temperature T_c, as in the case of photoinduced superconductivity (*30*, *31*).

REFERENCES AND NOTES

1. T. Sakudo, H. Unoki, *Phys. Rev. Lett.* **26**, 851–853 (1971).
2. A. Yamanaka *et al.*, *Europhys. Lett.* **50**, 688–694 (2000).
3. K. A. Müller, H. Burkard, *Phys. Rev. B* **19**, 3593–3602 (1979).
4. K. A. Müller, W. Berlinger, E. Tosatti, *Z. Phys. B Condens. Matter* **84**, 277–283 (1991).
5. J. G. Bednorz, K. A. Müller, *Phys. Rev. Lett.* **52**, 2289–2292 (1984).
6. M. Itoh *et al.*, *Phys. Rev. Lett.* **82**, 3540–3543 (1999).
7. D. G. Schlom *et al.*, *Annu. Rev. Mater. Res.* **37**, 589–626 (2007).
8. J. H. Haeni *et al.*, *Nature* **430**, 758–761 (2004).
9. M. Först *et al.*, *Nat. Phys.* **7**, 854–856 (2011).
10. T. F. Nova *et al.*, *Nat. Phys.* **13**, 132–136 (2017).
11. A. Subedi, A. Cavalleri, A. Georges, *Phys. Rev. B* **89**, 220301 (2014).
12. A. Subedi, *Phys. Rev. B* **95**, 134113 (2017).
13. A. P. Itin, M. I. Katsnelson, *Phys. Rev. B* **97**, 184304 (2018).
14. A. Cartella, T. F. Nova, M. Fechner, R. Merlin, A. Cavalleri, *Proc. Natl. Acad. Sci. U.S.A.* **115**, 12148–12151 (2018).
15. Supplementary materials.
16. M. Fiebig, V. V. Pavlov, R. V. Pisarev, *J. Opt. Soc. Am. B* **22**, 96–118 (2005) review.
17. M. Takesada, M. Itoh, T. Yagi, *Phys. Rev. Lett.* **96**, 227602 (2006).
18. U. Bianchi, W. Kleemann, J. G. Bednorz, *J. Phys. Condens. Matter* **6**, 1229–1238 (1994).
19. H. Uwe, T. Sakudo, *Phys. Rev. B* **13**, 271–286 (1976).
20. P. Zubko, G. Catalan, A. K. Tagantsev, *Annu. Rev. Mater. Res.* **43**, 387–421 (2013).
21. P. Zubko, G. Catalan, A. Buckley, P. R. L. Welche, J. F. Scott, *Phys. Rev. Lett.* **99**, 167601 (2007).
22. H. W. Jang *et al.*, *Phys. Rev. Lett.* **104**, 197601 (2010).
23. S. Orlov, A. Yariv, M. Segev, *Appl. Phys. Lett.* **68**, 1610–1612 (1996).
24. Y. Pochi, G. Claire, Eds., *Landmark Papers on Photorefractive Nonlinear Optics* (World Scientific, 1995).
25. A. Ohtomo, H. Y. Hwang, *Nature* **427**, 423–426 (2004).
26. C. H. Ahn, K. M. Rabe, J.-M. Triscone, *Science* **303**, 488–491 (2004).
27. L. Stojchevska *et al.*, *Science* **344**, 177–180 (2014).
28. M. Fiebig, K. Miyano, Y. Tomioka, Y. Tokura, *Science* **280**, 1925–1928 (1998).
29. A. Cavalleri *et al.*, *Phys. Rev. Lett.* **87**, 237401 (2001).
30. M. Mitrano *et al.*, *Nature* **530**, 461–464 (2016).
31. D. Fausti *et al.*, *Science* **331**, 189–191 (2011).
32. Y. L. Li *et al.*, *Phys. Rev. B* **73**, 184112 (2006).
33. P. Dore, G. De Marzi, A. Paolone, *Int. J. Infrared Millim. Waves* **18**, 125–138 (1997).

ACKNOWLEDGMENTS

We are grateful to T. Gebert for providing the beam propagation simulations. We thank A. Cartella for the help in building the OPA and K.Beyerlein for useful discussions. **Funding:** The research leading to these results received funding from the European Research Council under the European Union's Seventh Framework Programme (FP7/2007-2013)/ERC [grant agreement no. 319286 (QMAC)]. **Author contributions:** A.C. conceived the project together with T.F.N. T.F.N. and A.S.D designed the experiments and acquired and analyzed the data. M.F. developed the theoretical model and performed the DFT calculations. The manuscript was written by T.F.N. and A.C., with feedback from all coauthors. **Competing interests:** The authors declare no competing interests. **Data availability:** All data needed to evaluate the conclusions in the paper are present in the paper or the supplementary materials.

SUPPLEMENTARY MATERIALS

science.sciencemag.org/content/364/6445/1075/suppl/DC1
Materials and Methods
Supplementary Text
Figs. S1 to S14
Tables S1 to S3
References (*34*–*51*)

27 December 2018; accepted 20 May 2019
10.1126/science.aaw4911

Science

Metastable ferroelectricity in optically strained $SrTiO_3$

T. F. Nova, A. S. Disa, M. Fechner and A. Cavalleri

Science **364** (6445), 1075-1079.
DOI: 10.1126/science.aaw4911

Driving strontium titanate ferroelectric

Hidden phases are metastable collective states of matter that are typically not accessible on equilibrium phase diagrams. Nova *et al.* used infrared pulses to excite higher-frequency lattice modes that drive the crystal into a metastable ferroelectric phase, a phase that can persist for many hours. X. Li *et al.* used terahertz fields to drive the soft mode that moves the ions in the crystal into the positions they occupy in the new phase. The ferroelectric phase in this case was transient, lasting on the order of 10 picoseconds. Because these hidden phases can host exotic properties in otherwise conventional materials, the accessibility to and control of such hidden phases may broaden potential functionality and applications.

Science, this issue p. 1075, p. 1079